ELSEVIER

Journal of Nuclear Materials 289 (2001) 128–135

journal of nuclear materials

www.elsevier.nl/locate/jnucmat

# Hydrogen–damage interactions in yttria-stabilized zirconia

V. Shutthanandan *, S. Thevuthasan, J.S. Young, T.M. Orlando, W.J. Weber

*Environmental Molecular Sciences Laboratory, Pacific Northwest National Laboratory, P.O. Box 999, MSIN K8-93, Richland, WA 99352, USA*

**Abstract**

Hydrogen diffusion and accumulation in oxidized Zr($ZrO_2$) and oxide–metal interfaces lead to hydrogen induced cracking in Zr-based compounds that are extensively used in nuclear reactors. In this study, the interaction of hydrogen with irradiation damage in (0 0 1) single crystals of yttria-stabilized zirconia (Y–$ZrO_2$) has been investigated as a function of damage accumulation and temperature. Samples were irradiated with 40 keV hydrogen ions at a temperature of 120 K to ion fluences of $5 \times 10^{16}$ and $1 \times 10^{17}$ ions/cm$^2$, and isochronal experiments were performed in the temperature range from 300 to 770 K in 100 K steps. Damage accumulation and hydrogen profile measurements indicate unusual damage recovery behavior, pinning of hydrogen by damage, and surface deformation due to hydrogen blisters and bubbles. © 2001 Published by Elsevier Science B.V.

*PACS:* 61.85 +p; 61.72 Ji; 61.80 Jh

## 1. Introduction

Zirconium alloys are widely used in core structural components of water-cooled and water-moderated reactors due to zirconium's low neutron absorption cross-section. The oxidation of Zr alloys with steam, water, or radiolysis products of water leads to the nucleation and growth of hydride phases, which promote the stress corrosion cracking of cladding and other core structural components. Hydrogen embrittlement of Zr metals and Zr alloys has been extensively studied in the past [1–5], and it is believed that the hydrogen embrittlement in zirconium and its alloys occurs by penetration of hydrogen through the oxide films into the zirconium [6]. As such, it is important to understand hydrogen uptake through the oxides. A detailed understanding of hydrogen transport processes through the oxide film is required to clarify the mechanisms of hydrogen diffusion into the metals. Surface preparation, heat treatment, and oxide film thickness affect the hydrogen permeation properties in zirconium oxides [1]. In addition, the hydrogen transport through the oxide film depends on the size distribution and density of the intermetallic precipitates, and irradiation has a significant influence on the precipitates. Although the influence of intermetallic precipitates on hydrogen uptake through the oxide film has been addressed to some extent [5], systematic studies of hydrogen uptake into Zr alloys as a function of alloy composition, surface oxide thickness, and irradiation damage have not been performed. It has been reported that the hydrogen uptake is small for the fine precipitates compared to coarse precipitates in the oxide film [5]. Furthermore the ionization induced diffusion also a play an important role in the transport of hydrogen through oxides [7].

In another Zr–Nb 2.5% alloy and $ZrO_2$ study, about 40 keV deuterium was implanted into the material and the deuterium depth distribution was investigated using the $D(^3He, p)^4He$ nuclear reaction analysis (NRA) [8]. The results show that the $D(^3He, p)^4He$ NRA in conjunction with SIMS provides a means for quantitative depth profiling of deuterium. In general, a modest depth resolution and high accuracy in quantification can be achieved in NRA measurements, and these measurements are insensitive to matrix effects. Although SIMS measurements are sensitive to matrix effects, the spatial resolution and the sensitivity for hydrogen is relatively

* Corresponding author. Tel.: +1-509-376 2708; fax: +1-509-376 5106.

*E-mail address:* shuttha@pnl.gov (V. Shutthanandan).

0022-3115/01/$ - see front matter © 2001 Published by Elsevier Science B.V.
PII: S0022-3115(00)00692-9

high in SIMS measurements. In the present study, hydrogen NRA has been used to quantify the hydrogen in the material.

Radiation effects on Zr alloys using high energy protons and neutrons have been studied in the past [9–12]. Neutron irradiation studies [2] suggest that there is a significant change in hydrogen uptake in Zr alloys due to the irradiation-induced microstructural change in the material. Irradiation causes partial or full amorphization of $Zr(Fe,Cr)_2$ and $Zr_2(Fe,Ni)$ precipitates in the protective oxide layer of zirconium alloys. Because irradiation produces amorphous insulator particles [13], the electron transport properties of the oxide will change at some fluence. Since a potential gradient across the oxide increases, $H^+$ is expected to diffuse faster and further into the material.

Recently, Thevuthasan and co-workers [14] have demonstrated that hydrogen implantation followed by subsequent annealing can cleave single crystal oxide thin films with known thickness in $SrTiO_3$ (1 0 0) single crystal substrates. It is not clear whether this process can be utilized in many other oxide single crystals to generate thin oxide films, which can be effectively used in many applications. Hence, understanding the cleavage of thin films in yttria-stabilized zirconia single crystals is an additional benefit of this study. The current study investigates the effects of hydrogen implantation, implantation damage, and subsequent annealing in yttria-stabilized $ZrO_2$ (1 0 0) using Rutherford backscattering spectrometry in channeling geometry (RBS/C), NRA, and scanning electron microscopy (SEM).

## 2. Experimental procedure

Hydrogen implantation at 120 K to fluences of 40 keV $5.0 \times 10^{16}$ and $1.0 \times 10^{17}$ $H^+/cm^2$ was carried out on yttria-stabilized $ZrO_2$ (1 0 0) single crystals at Implant Science Corporation. After implantation, the samples were shipped to Pacific Northwest National Laboratory (PNNL) and stored in a desiccator for 3–4 months prior to the annealing experiments. The sample dimensions were 1.0 cm × 1.0 cm × 1.0 mm, and a conventional alumel–chromel thermocouple was placed on a corner of the sample surface and held by a Ta clip during the RBS/C experiments. The damage recovery experiments were carried out using the accelerator facility within the Environmental Molecular Sciences Laboratory (EMSL) at PNNL. The accelerator facility and the end stations are described in detail elsewhere [15]. Isochronal annealing of the hydrogen implanted Y–$ZrO_2$ single crystals was performed for 20 min in high vacuum applying at each temperature step. The annealing temperatures were varied from 370 to 870 K at 100 K intervals with ±5 K uncertainty in the temperature. After each annealing step, the sample was cooled down, and the RBS/C and hydrogen NRA measurements were carried out at a sample temperature of 300 K using 2.0 MeV $He^+$ and 6.40–8.04 MeV $F^{3+}$ ions. The RBS/C spectra were collected using a silicon surface barrier detector at a scattering angle of 150°. The hydrogen NRA measurements were performed using the resonant $^1H(^{19}F, \alpha\gamma)^{16}O$ reaction [16]. During the NRA measurements, the sample was in kept in random orientation and a 50 mm × 100 mm bismuth germanium oxide (BGO) detector was used to collect the gamma rays produced by the reaction. The hydrogen quantification was calibrated against the hydrogen measurements from $1 \times 10^{17}$ $H^+/cm^2$ implanted SiC single crystal. Sample heating during these measurements increased the temperature for some measurements to 325–350 K. At the end of 770 K annealing, the samples were removed from the ion scattering chamber, and the SEM measurements were performed using LEO 982 SEM instrument.

## 3. Results and discussion

The accumulation of damage and subsequent recovery in the hydrogen-implanted Y–$ZrO_2$ (1 0 0) single crystals was studied primarily using the damage peak profiles, the surface peak (SP) areas, and the minimum yields ($\chi_{min}$) in the RBS/C measurements. By measuring the hydrogen depth profile after every annealing step, it is possible to correlate the hydrogen in some ways to thermal recovery behavior of defects generated during irradiation. Furthermore, the SEM measurements from these samples can be used to study the morphology changes in the surface as the consequent of hydrogen interaction with the material and the defects in the material.

In Fig 1 we present the channeling spectra measured from the irradiated and virgin regions of the crystal (implanted with $1.0 \times 10^{17}$ $H^+/cm^2$) for several annealing temperatures along with a random spectrum. The arrows in the figure indicate the energy positions expected for backscattering from Zr and O atoms at the surface as well as from the damage region. Only the RBS/C spectra from the irradiated region for 300, 370, 470 and 770 K annealing are shown to minimize the interference between different spectra. Although the ion irradiation produced damage on both the Zr and O sublattices, only the damage created on the Zr sublattice is followed. The damage produced on the Zr sublattice after the implantation is rather dilute, and the peak due to the damage is broad, perhaps due to diffusion at the implantation temperature (300 K RBS/C spectrum). However, as shown in the figure, the damage peak appears to be narrow and well defined with increasing annealing temperatures.

The hydrogen concentration profiles, determined using the hydrogen NRA, are presented in Fig. 2 for

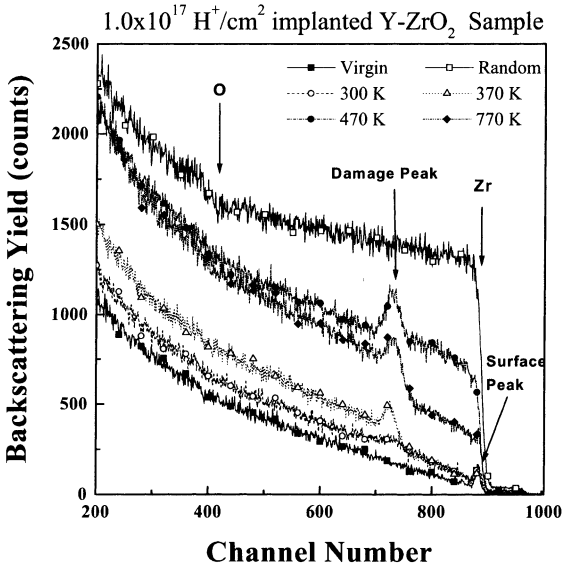


Fig. 1. Ion scattering/channeling spectra for 2 MeV $He^+$ ions on virgin and $1 \times 10^{17}$ $H^+/cm^2$ implanted Y–$ZrO_2$ (1 0 0) single crystal sample, for selected isochronal annealing temperature as indicated in the figure. The energies of the Zr, O surface peak as well as the damage peak of the Zr are indicated by the arrows.

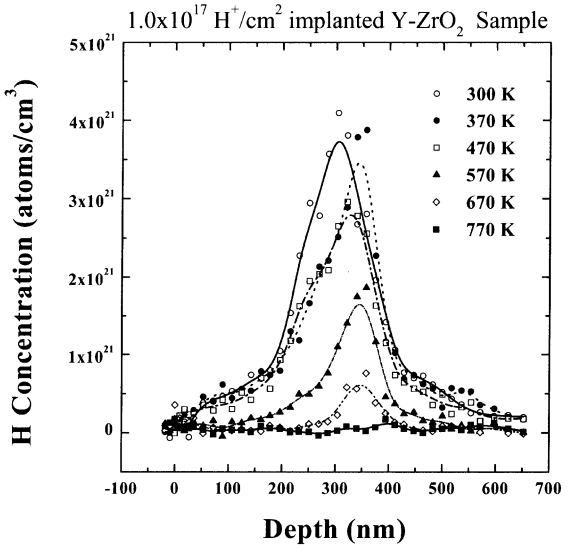


Fig. 2. The hydrogen depth profiles measured by the resonant $^1H(^{19}F, \alpha\gamma)^{16}O$ nuclear reaction for the $1 \times 10^{17}$ $H^+/cm^2$ implanted Y–$ZrO_2$ (1 0 0) single crystal sample are presented. The profiles were taken after 300, 370, 470, 570, 670 and 770 K isochronal annealing.

annealing up to 770 K. The as-implanted hydrogen profile is peaked at a depth of 300 nm, and a small shoulder is visible around 150 nm from the surface. The integrated area under each individual curve will give the total amount of hydrogen accumulated in the sample. Before any heat treatments, the integrated hydrogen dose appears to be $0.72 \times 10^{17}$ $H^+/cm^2$, which is significantly less than the implanted hydrogen ion dose of $1.0 \times 10^{17}$ $H^+/cm^2$. It appears that some hydrogen was lost by diffusing out the surface of the sample and/or into the bulk during the sample storage at EMSL. The broad tails on both sides of hydrogen profiles confirm the hydrogen diffusion from the implanted region. Annealing the sample to 370 K resulted in an increase in the backscattering yield from the Zr sublattice near the damage peak. This suggest that there is some increased disordering of Zr atoms during annealing due to the possible interaction of H with the structure or the formation of defect clusters or bubble nuclei. The hydrogen profile data shows a peak shifted towards larger depth (350 nm) with almost the same hydrogen diffusion towards the surface as the room temperature hydrogen profile.

Although the damage generated in the Zr sublattice was not significantly increased near the damaged peak position at 470 K annealing, there was a significant increase in the dechanneling from the near-surface region. The channeling spectrum looks similar to the random spectrum with the height near the surface region at approximately 50% of the random height. One possibility for the unusual increase in the backscattering yield from the near surface region is the strain and deformation induced by the formation of hydrogen defect clusters or hydrogen blisters in this region after annealing at 470 K. However, there is no significant difference in the damage peak compared to the damage peak after 370 K annealing. This indicates that the damaged region is not significantly altered due to the deformation of the surface region. Further annealing at 570 and 670 K significantly reduces the amount of hydrogen in the analysis region. The aligned spectra after these annealing cycles (not shown in Fig. 1) show a slight decrease in the backscattering yield from the deformed region. However, no significant differences were observed in the damage peak. Further annealing at 770 K reduced the total amount of hydrogen to the background level. The damage, including the deformation of the surface region, appears to decrease as a result of this annealing. Although virtually no hydrogen is present in the system, within the detection limits, some deformation of the surface region still remains after annealing at 770 K.

SEM measurements were carried out on the 770 K annealed sample to understand the morphology and microstructural changes in the material due to hydrogen interaction with the material and defects during the annealing. SEM images obtained from an unirradiated region and an irradiated region after 770 K annealing are shown in Figs. 3(a) and (b), respectively. The irradiated region shows blisters and bubbles of several micron diameters. It is also clear from the figure that some

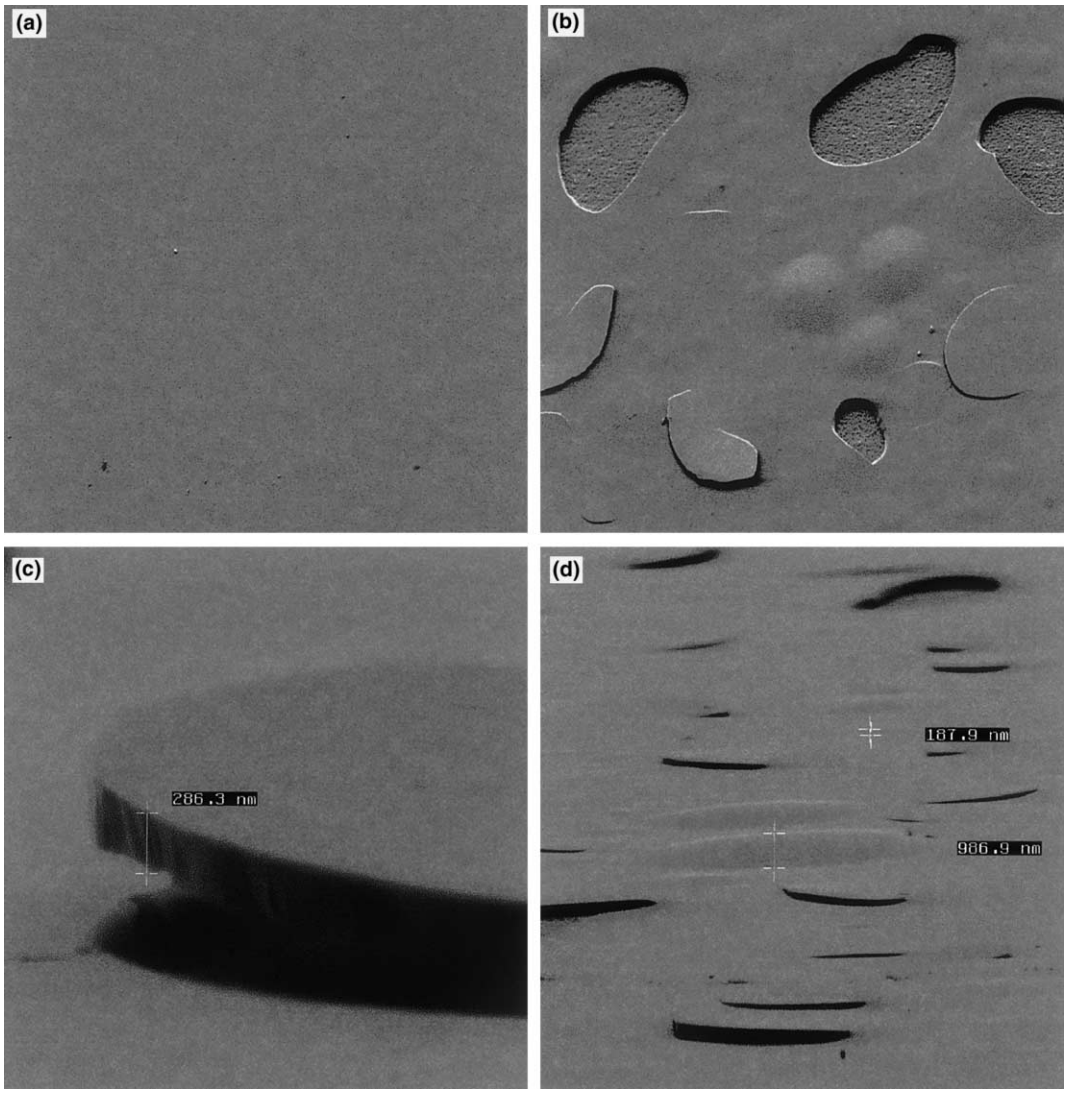


Fig. 3. SEM images from a virgin and $1 \times 10^{17}$ $H^+/cm^2$ implanted Y–$ZrO_2$ (1 0 0) single crystal sample: (a) virgin; (b) irradiated and anneal sample after 770 K annealing; (c) side view of the single blister cap and (d) side view of the bubbles and the blisters.

of the hydrogen blisters are ruptured during the annealing. Fig. 3(c) shows the side view of an individual ruptured blister cap. The average thickness of the blister cap appears to be in the range 270–350 nm, which is close to the range of the implanted hydrogen in Y–$ZrO_2$. However, the size of the un-ruptured bubbles that are still intact after 770 K annealing (Fig. 3(d)) seems to be varying from 100 to 1000 nm. These blisters and bubbles are responsible for the deformation of surface region. As a result, an increase in the backscattering yield was observed in the channeling spectra taken after annealing at 470, 570, 670 and 770 K.

It is possible that the tiny hydrogen particles generated during the initial annealing temperature (up to 370 K) might have combined together to form relatively larger bubbles during annealing at 470 K. This is evident from Fig. 1, where unusually high dechanneling was observed after annealing the sample at 470 K. Eventually, due to the high $H_2$ gas pressure in the bubbles, some of the bubbles ruptured and blisters formed during the high temperature annealing. This is evident from Fig. 2, where considerable amount of hydrogen (about 30 %) left the sample after 570 K of annealing. Since not all the hydrogen has left the sample, it is possible that some of the bubbles formed at 470 K are still intact (unruptured) even after the high temperature annealing. In addition, during the high temperature annealing (above 570 K), the residual hydrogen might have an additional

diffusion path, through the ruptured blisters, to leave the sample. Because of this additional diffusion path some of the hydrogen bubbles are intact.

In order to understand the effect of implantation dose on damage accumulation and subsequent thermal recovery, we have repeated similar measurements on $5.0 \times 10^{16}$ $H^+/cm^2$ implanted Y–$ZrO_2$ sample. The RBS/C and hydrogen measurements from this sample are shown in Figs. 4 and 5, respectively. The initial (as-implanted) damage on the Zr sublattice is slightly higher than that of the high fluence ($1 \times 10^{17}$ $H/cm^2$) and the hydrogen depth profile shows a broad peak (Fig. 5) with the peak position around 350 nm from the surface. As in the case of higher dose, the amount of hydrogen in the sample was less compared to the implantation dose possibly due to hydrogen loss from the implanted region. No significant difference was observed in the channeling spectrum after 370 K annealing (Fig. 4). After 470 K annealing, a slight decrease in the backscattering yield across the penetration depth of the implanted hydrogen was observed. Although dechanneling in the surface region is still much higher compared to the channeling spectrum from virgin sample, the damage peak has been virtually removed during this annealing. Similar appearance between the channeling spectra after annealing at 470 and 770 K suggests that there is no significant decrease in the dechanneling as a function of temperature.

The relative disorder at the damage peak in both low (open circles) and high dose (closed circles) irradiated

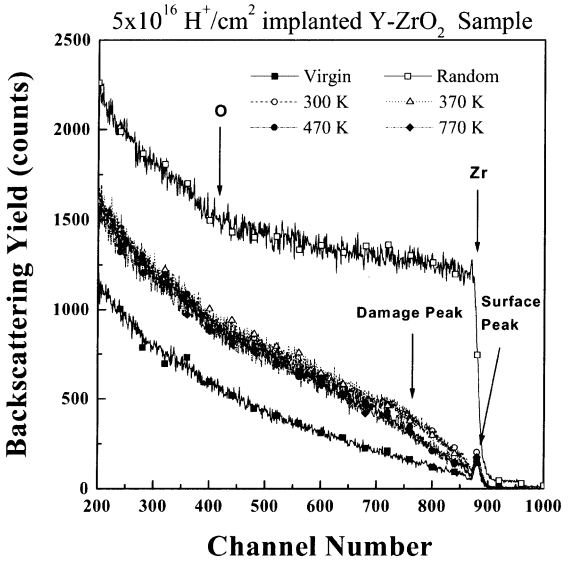


Fig. 4. Ion scattering/channeling spectra for 2 MeV $He^+$ ions on virgin and $5 \times 10^{16}$ $H^+/cm^2$ implanted Y–$ZrO_2$ (1 0 0) single crystal sample, for selected isochronal annealing temperature as indicated in the figure. The energies of the Zr, O surface peak as well as the damage peak of the Zr are indicated by the arrows.

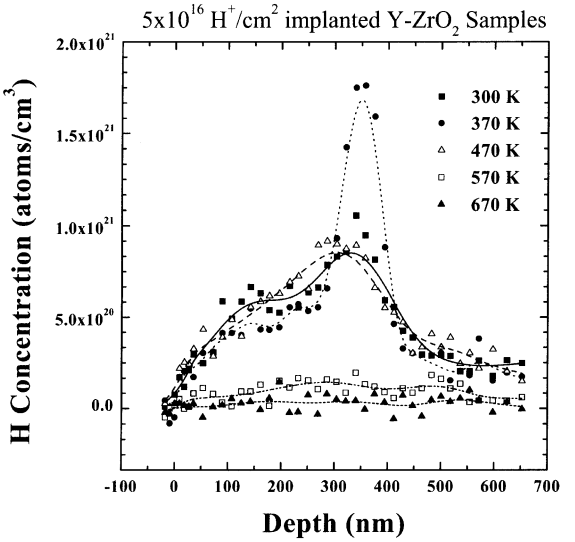


Fig. 5. The hydrogen depth profiles measured by the resonant $^1H(^{19}F, \alpha\gamma)^{16}O$ nuclear reaction for the $5 \times 10^{16}$ $H^+/cm^2$ implanted Y–$ZrO_2$ (1 0 0) single crystal sample are presented. The profiles were taken after 300, 370, 470, 570, 670 and 770 K isochronal annealing.

samples as a function of annealing temperature is shown in Fig. 6(a). The relative disorder was calculated as the ratio between damage peak height after the background subtraction for the dechanneling effects to the random height at the damage peak position. The solid lines are intended to guide the eye. It is clear from this figure that the damage production and the subsequent recovery are different for these two samples. Even though, the initial damage is higher in the low dose sample, the high dose sample shows a rapid damage increase as the annealing temperature increases up to 470 K. In fact, the low dose sample started to recover its damage right after the first annealing. After annealing to 770 K, although the dechanneling in the surface region is still high, the recovery is virtually complete in the low dose sample. Although the high dose sample shows some kind of damage recovery, the damage caused by the hydrogen interaction is still very high even after annealing at 770 K.

Fig. 6(b) shows the surface disorder as a function of annealing temperature for high and low dose samples, respectively. We define the surface disorder as the ratio of SP area to the integrated random yield within the same energy window. In the low dose sample, no significant variations in the surface disorder was observed as a function of annealing temperature up to 770 K within the experimental uncertainties (less than 5%). On the other hand, the high dose sample shows significant variations in the surface disorder as a function of annealing temperature. After annealing at 370 K, there is not much increase in surface disorder in the high dose sample as in the case of low dose sample. However, after

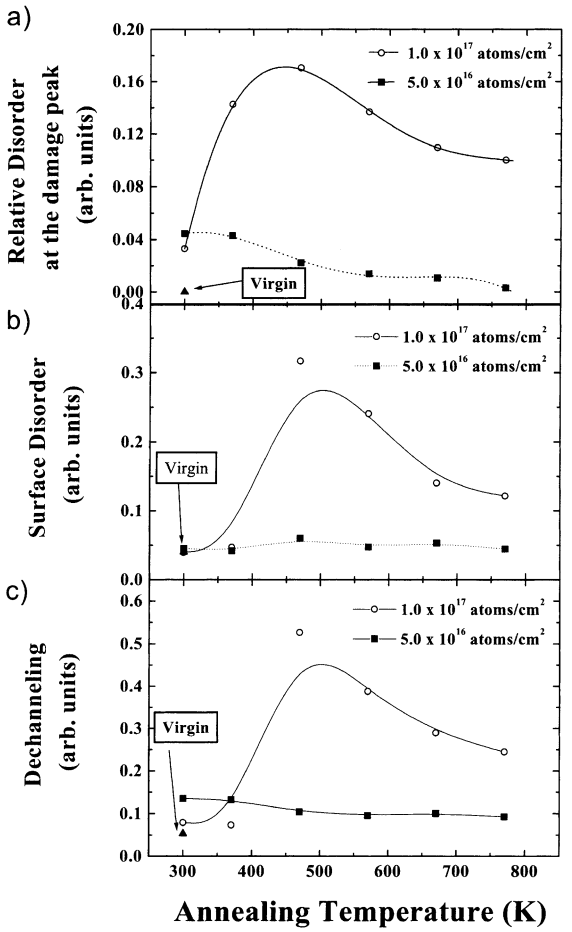


Fig. 6. Damage accumulation and the thermal recovery behavior of the hydrogen implanted Y–$ZrO_2$ (1 0 0) single crystal sample for $5.0 \times 10^{16}$ H/cm$^2$ and $1.0 \times 10^{17}$ H/cm$^2$ doses as a function of annealing temperatures: (a) relative disorder at the damage peak; (b) surface disorder and (c) dechanneling contribution to the backscattering yield.

annealing at 470 K the high dose sample shows significant increase in the surface disorder as seen in Fig. 6(b). This sudden increase in the surface disorder has been caused by the deformation of the surface region due to formation of tiny hydrogen bubbles. The surface disorder appears to decrease as a result of further annealing. However, the surface disorder after 770 K annealing is still much higher than the virgin sample possibly because of the remnants of the ruptured blisters in the surface region. Similar trends were observed in the dechanneling contribution to the backscattering yield as a function of annealing temperature for both low and high dose samples and the results are shown in Fig. 6(c). Dechanneling in the low dose sample appears to be decreasing as a function of annealing temperature. On the other hand, the variations in the dechanneling in the high dose sample are similar to the variations in the surface disorder.

The total amount of hydrogen remaining in both the low dose (closed circles) and high dose (open circles) samples after each annealing step is shown in Fig. 7. The solid lines are intended to guide the eye. Clearly, both samples lost most of the hydrogen after annealing at 570 K. However, up to 470 K annealing, the hydrogen loss is gradual in high dose sample while there is no significant hydrogen loss in the low dose sample. Almost all the hydrogen was removed during the annealing at 570 K in the low dose sample. Although significant amount of hydrogen was removed in the high dose sample during the 570 K annealing, a considerable amount of hydrogen still left in the sample after annealing at 670 K. It is possible that some of the hydrogen atoms or molecules are trapped in the bubbles for the high dose sample that might have slow down the hydrogen diffusion. Even though, the hydrogen depth profiles (in Fig. 5) are different from the low dose sample up to 470 K of annealing, the total dose of the hydrogen atoms in these three profiles are nearly identical. This suggests that the hydrogen atoms or molecules are loosely bonded to the damage regions in the low dose case. On the other hand, the hydrogen atoms or molecules in the high dose sample are tightly bonded to the damage region, as it is evident from Figs. 5 and 7.

SEM images obtained from an unirradiated region and an irradiated region in the low dose sample after 770 K annealing is shown in Fig. 8. Since there is no significant difference between both of these SEM images, it

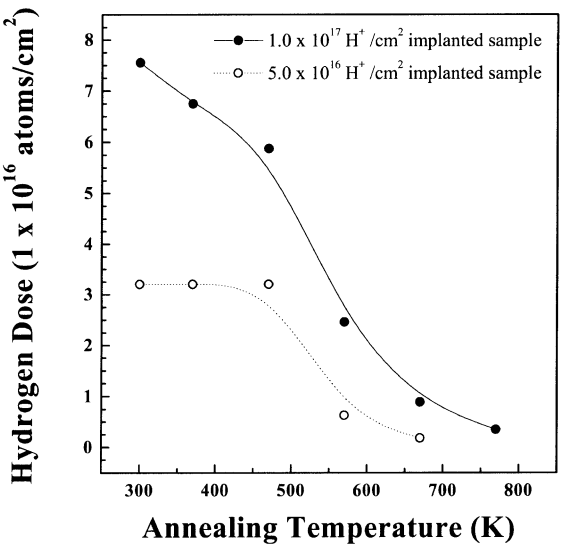


Fig. 7. Total number of hydrogen remains in the sample after the annealing as a function of annealing temperature for both low (open circles) and high (closed circles) dose samples. Solid lines are provided to guide the eye.

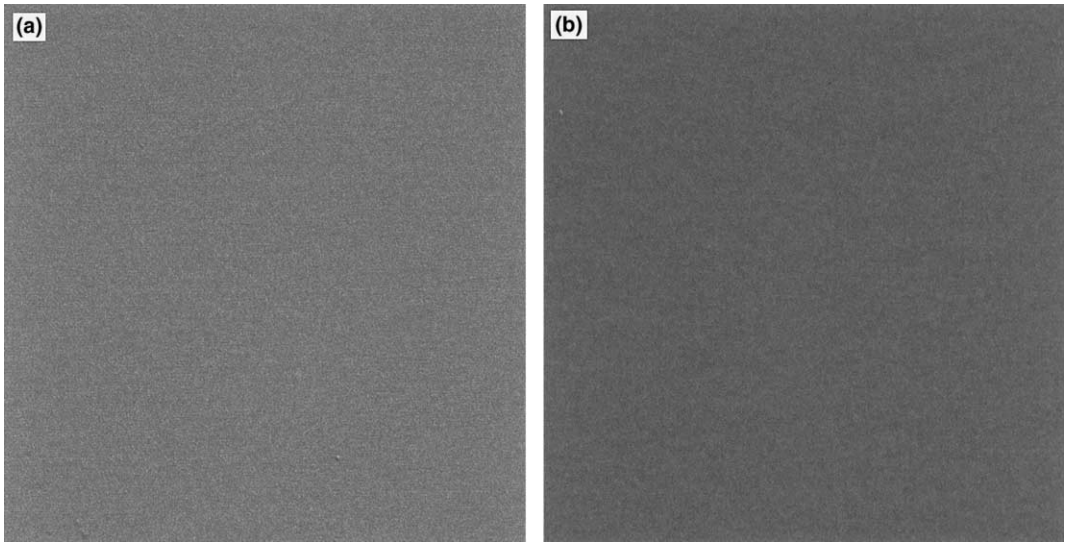


Fig. 8. SEM images from a virgin and $5 \times 10^{16}$ $H^+/cm^2$ implanted Y–$ZrO_2$ (1 0 0) single crystal sample: (a) virgin and (b) irradiated and anneal sample after 770 K annealing.

is clear that the surface morphology of the low dose sample was not altered during the annealing process. Contrary to the case of high dose sample, it appears that the hydrogen left the sample without making any significant damage in the surface region during the annealing. In a previous study by Thevuthasan and coworkers [14], it was shown that cleavage of thin film occurs in a $5.0 \times 10^{16}$ $H^+/cm^2$ irradiated sample and remnant of blisters appeared in the surface region of a $1.0 \times 10^{17}$ $H^+/cm^2$ irradiated sample during the annealing. Although similar blisters and deformations were observed for the high dose sample in the present work, any indications of cleavage of thin films on yttria-stabilized zirconia were not observed for the low dose. Further studies are necessary to determine the range of doses that can cause thin film cleaving in yttria-stabilized zirconia.

## 4. Conclusions

Damage accumulation and thermal recovery processes in 40 keV H implanted yttria-stabilized zirconia single crystals were investigated using RBS/C measurements for two different doses ($0.5 \times 10^{17}$ and $10 \times 10^{17}$ atoms/$cm^2$). The hydrogen quantification in the sample was performed using the $^1H(^{19}F, \alpha\gamma)^{16}O$ NRA. The surface morphology and the microstructures were analyzed using SEM. In the case of high dose sample, annealing at 470 K resulted in an increase of relative disorder, surface disorder and dechanneling across the penetration depth of the implanted region. Hydrogen bubbles were formed after annealing at 470 K and some of these bubbles were ruptured after further annealing. The SEM results show that remnant damage and deformation of surface region is still visible after 770 K annealing. On the other hand, the low dose sample shows much smaller surface disorder and damage accumulation as a consequence of annealing. No evidence of bubbles formation or ruptured blisters was observed in this sample after the annealing. The hydrogen depth profile measurements performed after 570 K annealing suggests that both samples lost most of the hydrogen at this temperature. The high dose sample appears to lose hydrogen at a slower rate than the low dose sample presumably due to the strong interaction with the damage regions.

## Acknowledgements

This research was supported by the Division of Materials Sciences, Office of Basic Energy Sciences, and the Environmental Management Science Program through Office of Environment, US Department of Energy. The experiments were performed at the EMSL, a national scientific user facility located at PNNL and supported by the US Department of Energy's, Office of Biological and Environmental Research. PNNL is a multi-program national laboratory operated for the US DOE by Battelle Memorial Institute under contract No. DE-AC06-76RLO 1830. The authors gratefully acknowledge helpful suggestions from Dr W. Jiang. We also grateful for the technical assistance of Evan M. Adams, Chad Cooper, and Chris Melendrez.

## References


[1] E.A. Gulbranson, K.F. Andrew, J. Electrochem. Soc. 101 (1954) 348.
[2] D.O. Northwood, U. Kosasih, Int. Met. Rev. 28 (1983) 92.
[3] M.P. Puls, J. Nucl. Mater. 165 (1989) 128.
[4] San-Qiang Shi, M.P. Puls, J. Nucl. Mater. 218 (1994) 30.
[5] Yuji Hantano, Kanetsugu Isobe, Ryuji Hitaka, Masayasu Sugisaki, J. Nucl. Sci. Technol. 33 (1996) 944.
[6] T. Smith, J. Nucl. Mater. 18 (1966) 323.
[7] S.J. Zinkle, Microstructure evolution during irradiation, in: I.M. Robertson (Ed.), MRS Symposium Proc., vol. 43a, Materials Research Society, Pittsburgh, 1997, p. 667.
[8] W.N. Lennard, G.R. Massoumi, P.F.A. Alkemade, I.V. Mitchell, N.S. McIntyre, R.D. Davidson, Nucl. Instrum. and Meth. B 73 (1993) 203.
[9] C.E. Coleman, P.C.K. Chow, C.E. Ells, M. Griffiths, E.F. Ibrahim, S. Sagat, Effects of radiation on materials, in: R.E. Stoller, A.S. Kumar, D.S. Gelles (Eds.), 15th International Symposium, ASTM STP 1125, American Society for Testing and Materials, Philadelphia, 1992, p. 318.
[10] S.T. Mahmood, S.A. Hussein, P.S. Godsvarti, K.L. Murty, Effects of radiation on materials, in: R.E. Stoller, A.S. Kumar, D.S. Gelles (Eds.), 15th International Symposium, ASTM STP 1125, American Society for Testing and Materials, Philadelphia, 1992, p. 337.
[11] J.-J. Kai, C.-H. Tsai, W.-F. Hsieh, Effects of radiation on materials, in: R.E. Stoller, A.S. Kumar, D.S. Gelles (Eds.), 15th International Symposium, ASTM STP 1125, American Society for Testing and Materials, Philadelphia, 1992, p. 355.
[12] V.I. Shcherbak, A.P. Pinchuk, V.P. Tarasikov, Sov. At. Energy 71 (1991) 697.
[13] D.G. Franklin, P.M. Lang, Zirconium in the nuclear industry, in: C.M. Eucken, A.M. Garde (Eds.), Ninth International Symposium, ASTM STP 1132, American Society for Testing and Materials, Philadelphia, 1991, p. 3.
[14] S. Thevuthasan, W. Jiang, W.J. Weber, Appl. Phys. Lett., submitted.
[15] S. Thevuthasan, C.H.F. Peden, M.H. Engelhard, D.R. Baer, G.S. Herman, W. Jiang, Y. Liang, W.J. Weber, Nucl. Instrum. and Meth. A 420 (1999) 81.
[16] J.R. Tesmer, M. Nastasi (Eds.), Handbook of Modern Ion beam Materials Analysis, Materials Research Society, 1995.